ELSEVIER

Nuclear Physics A576 (1994) 138–156

NUCLEAR PHYSICS A

Angular and velocity analysis of the three-fold events in the Xe + Cu reaction at 45 MeV/u

M. Bruno, M. D'Agostino, M.L. Fiandri, E. Fuschini, L. Manduci, P.F. Mastinu, P.M. Milazzo

Dipartimento di Fisica dell'Università and Istituto Nazionale di Fisica Nucleare, Bologna, Italy

F. Gramegna

Istituto Nazionale di Fisica Nucleare, Laboratori Nazionali di Legnaro, Legnaro, Italy

A.M.J. Ferrero [1], F. Gulminelli, I. Iori, A. Moroni, R. Scardaoni

Dipartimento di Fisica dell'Università and Istituto Nazionale di Fisica Nucleare, Milano, Italy

P. Buttazzo, G.V. Margagliotti, G. Vannini

Dipartimento di Fisica dell'Università and Istituto Nazionale di Fisica Nucleare, Trieste, Italy

G. Auger, E. Plagnol [2]

Laboratoire Nationale GANIL, Caen, France

Received 3 August 1993; revised 17 February 1994

Abstract

An analysis of the angular and velocity distributions of the intermediate mass fragments produced in the reaction Xe + Cu at 45 MeV/u is presented. Events coming from central collisions are selected and compared with predictions of different models based on a statistical deexcitation of an equilibrated source. The angular and velocity correlations show that the experimental production of three nearly-equal mass fragments cannot be explained by a sequential binary decay and is compatible with a multifragmentation mechanism.

[1] On leave from the Comision Nactional Energia Atomica, Argentina.
[2] Present address: IPN Orsay, France.

SSDI 0375-9474(94)00142-A

Key words: Nuclear reactions Cu(^{129}Xe, X), $E = 45$ MeV/nucleon; measured intermediate mass fragments; deduced correlation to impact parameters. Multi-fragmentation models comparison.

1. Introduction

To investigate the decay mechanisms of very hot nuclei produced in heavy-ion reactions it is essential to study the collisions according to the impact parameter in order to avoid a mixing of different exit channels. Only by selecting events coming from central collisions one can observe, at intermediate energies, if a critical phenomenon like a phase transition [1,2] occurs; moreover, comparison between experimental data and theoretical predictions are meaningful for measurements capable of selecting narrow ranges of impact parameters.

An observable used extensively [3] to evaluate the impact parameter is the multiplicity of charged particles; other observables, as the angular distributions of the intermediate mass fragments (IMFs, $Z > 2$) and their emission velocities, have also been used for similar purposes [4,5].

In a previous paper [6] first results on the charge correlation of three IMFs emitted in the ^{129}Xe + ^{nat}Cu reaction at 45 MeV/u were reported: a relatively high probability for the emission of three fragments of nearly the same charge was observed, not in agreement with a sequential binary statistical decay [7] of the sources formed in the reaction.

This work is devoted to a deeper characterization of the three-fold events, in order to select the most central collisions and to investigate, looking for correlations on charge, velocity and angular distributions, if they originate from a simultaneous multifragment decay of an equilibrated source.

The topology of the fragment emission in events following a sequence of binary decays is strongly influenced by the first decay step, in which two prefragments move back to back in the rest frame of the decaying system. The sequential two-body decays of these excited prefragments then result in final-state emission patterns that are elongated in the momentum space. Multifragmentation reactions, involving a more rapid explosion of excited nuclei, are, on the contrary, expected to result in more isotropic fragment-emission patterns. The study of the experimental distributions of the relative velocities and angles [8] between pairs of fragments in high-multiplicity events can thus allow for a better understanding of the deexcitation mechanism.

After a short description of the experimental setup, the inclusive data as well as the predictions of a coupled dynamical and sequential decay model are discussed. The angular and velocity correlations for coincident fragments, selected for the centrality of the reaction, are then presented and compared to the predictions of a multifragmentation model [2].

2. Experimental setup

The apparatus and the details of the measurement have been described elsewhere [6,9]; we recall here only the main features.

The experiment was performed using the MULTICS apparatus in the scattering chamber NAUTILUS at the GANIL Laboratory.

An ^{129}Xe beam from the coupled cyclotrons impinged on a target of ^{nat}Cu (thickness ≈ 2 mg/cm^2). In order to measure absolute cross sections, the beam current was integrated in a Faraday cup. An ^{197}Au target (thickness ≈ 0.8 mg/cm^2) was used for calibration and normalization purposes.

The MULTICS apparatus is an array of 48 identical modules with front surface tangent to a sphere (with radius 50 cm) centered in the target; the array covers the angular range 3°–23° with a geometrical efficiency of 72%. Each module consists of a three-detector telescope: an axial ionization chamber (IC length 8.5 cm), a two-dimensional position-sensitive solid-state detector (Si), 500 μm thick, and a CsI scintillator, 25 mm thick and coupled to a photodiode, used as E detector for charged particles that punch through the first two elements of the telescope.

Operating at 200 mbar of CF_4, the energy threshold is ≈ 2.5 MeV/u, corresponding to a velocity ≈ 2.2 cm/ns. The IC–Si telescopes can stop from 8.5 MeV/u He ions to 40 MeV/u Xe ions.

The overall energy resolution is better than 2%, the angular resolution ranges from 0.1° to 0.3° [10] and the atomic numbers can be identified up to $Z = 56$.

Great effort has been devoted to the detector calibration, especially for the CsI crystals: specific measurements were performed at the Berkeley Laboratories [11] for an accurate analysis [12] of the nonlinear light-output dependence on the energy and the charge of the incident ions.

The trigger was given by the $\frac{45}{48}$ Si detectors working during the measurement. Due to some technical problems, the Z identification has been made only for the telescopes ($\approx 50\%$) with low-energy threshold; the angular coverage considered in the following analysis is $\theta > 5.5°$. Thus, since for this reaction the grazing angle is less than 2°, most of the events coming from peripheral reactions were not detected, being the projectile-like fragments outside the acceptance of the apparatus.

3. Inclusive data

The experimental cross sections as a function of the IMF ($Z > 2$) multiplicity and the inclusive Z cross sections are presented in Fig. 1. The statistical uncertainty is negligible and an error of the order of 10% can be associated to the experimental cross sections, due to the normalization to the Rutherford cross section.

A nonnegligible contribution of high-multiplicity events has been found, not reproduced by a statistical-binary-decay model (Gemini code [7]) with inputs

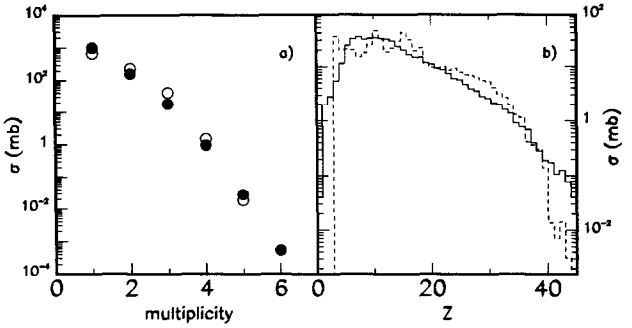

Fig. 1. (a) Cross sections as a function of the multiplicity for the overall apparatus. The full circles are the experimental results, the open ones the predictions by the coupled dynamical and statistical approach, filtered by the acceptance of the apparatus. (b) Cross sections as a function of the charge of the detected IMFs. The continuous line shows the experimental results, the dashed one the model predictions filtered by the acceptance of the low-threshold detectors. No normalization has been applied.

obtained from the incomplete-fusion systematics, which underestimates the cross sections by roughly a factor 10 [6].

Preliminary information on the dynamics of the reaction can be obtained by plotting the parallel versus the transverse component of the velocity for different Z values (see Fig. 2). The velocity of each fragment has been extracted from the measured energy and charge values, assuming for the ion mass the expression [13]

$$A = 2.08Z + 0.0029Z^2. \tag{1}$$

In agreement with results obtained in similar reactions [5,14], the so-called Coulomb rings, typical of lower energies [7], are not formed. This indicates that the IMFs are produced by sources with velocities ranging from a low value, corresponding to a quasi-target residue to a higher one, typical of a quasi-projectile.

Since the gross features of the data, as the inclusive cross sections, mainly depend on the weight of the impact parameters, we took into account the entrance-channel dynamics, coupling [15] the Gemini code to a dynamical model based on the BNV equation [6].

The dynamics of the interaction has been followed up to a time of the order of 80–100 fm/c, when a statistical equilibrium has been reached. The excited-system information (mass, excitation energy, intrinsic angular momentum and laboratory velocity) are shown in Fig. 3, as obtained by a coalescence model [15] of the mean one-body distribution in the phase space. A single excited source is obtained at small impact parameters ($b \leqslant 2$), whereas two different sources have been obtained for increasing impact parameter: a "big" source, close in mass to the projectile and with a velocity approaching the beam velocity for increasing b, and a "small" one, close to the target and approaching zero velocity for increasing b.

It is important to note that theoretical predictions must be filtered, event by event, through the detector acceptance, in order to allow meaningful comparison

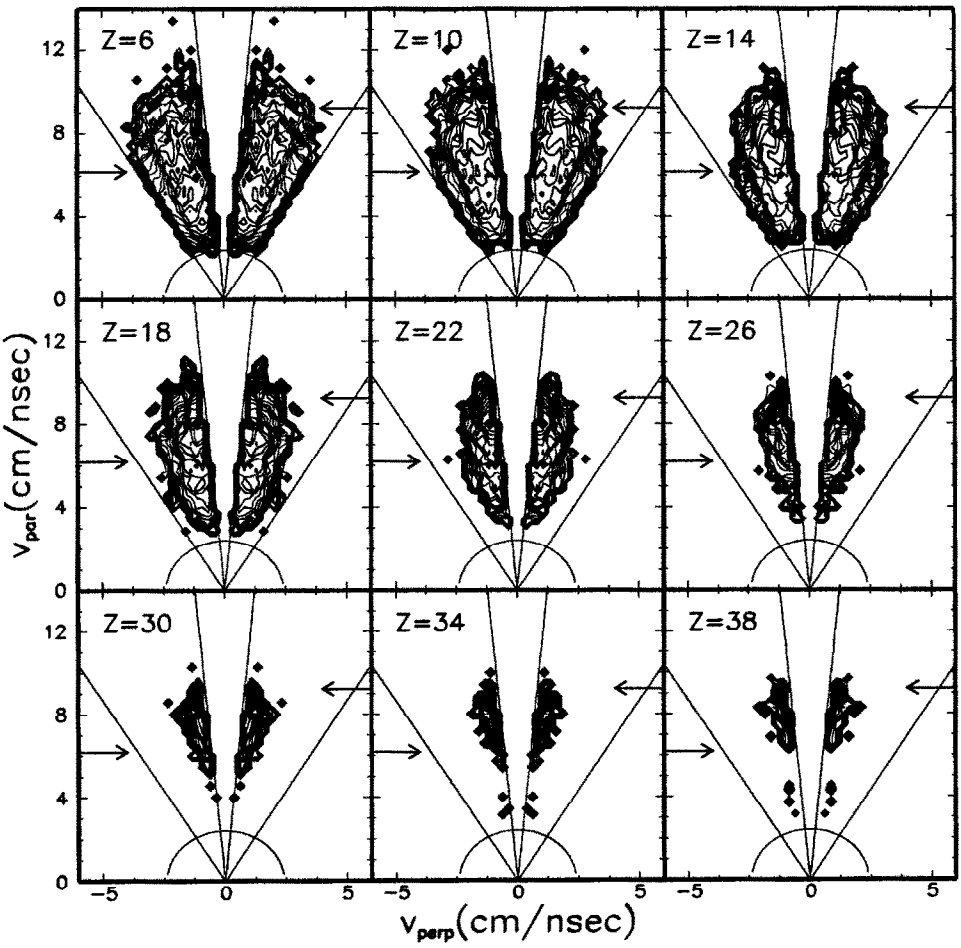

Fig. 2. Logarithmic contour plots of the experimental parallel ($v_{\parallel}$) versus perpendicular ($v_{\perp}$) velocity for inclusive events. The upper arrow corresponds to the velocity of the beam and the lower one to the velocity of a source obtained by complete fusion. The contour lines (15) are equispaced and the associated values increase following the colour scale black, red, green, violet.

with the inclusive and exclusive data. An accurate software replica of the experimental apparatus is then necessary, through which the generated events are filtered before comparison with the experimental events. This software must include a realistic treatment of the geometrical inefficiencies, the particle-kinetic-energy threshold and the particle energy loss in inactive regions [16].

The results of the calculations, weighted on the impact-parameter and filtered by the overall acceptance of the apparatus, well reproduce the inclusive data without any normalization:

(1) the predicted total cross section for fragment production of any multiplicity is 0.995 b and the experimental value is 1.23 b;

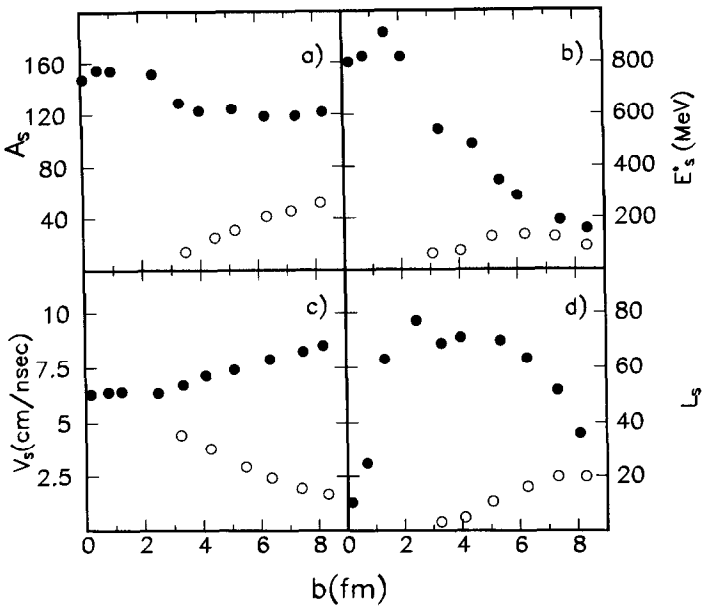

Fig. 3. Characteristics of the *sources* for the Xe+Cu reaction at 45 MeV/u versus the impact parameter value; (a) mass, (b) excitation energy, (c) laboratory velocity, (d) angular momentum ($\hbar$).

(2) the experimental cross sections as a function of the IMF ($Z > 2$) multiplicity and the inclusive Z cross sections, as can be seen from Fig. 1, are in good agreement with the experimental ones;

(3) the cross section $d^2\sigma/dv_{\|}\,dv_{\perp}$, predicted by coupling of BNV + Gemini, filtered by the overall acceptance of the apparatus, agrees with the experimental one, especially for $Z > 10$ (see Fig. 4).

The agreement between inclusive data and calculations, indicates that the entrance-channel characteristics, like the masses, charges, excitation energies and angular momenta of the sources, are correctly calculated using the BNV dynamics and that the filtering procedure takes well into account the overall acceptance. No definite conclusions, however, on the deexcitation mechanism of the hot systems formed in central collisions can be drawn from the inclusive data, due to the small contribution to the cross sections of small impact parameters. To investigate this point it is necessary to estimate the centrality of the events and to consider observables more related to the decay mode of the emitting sources.

A first indication on the range of the impact parameters contributing to the measured inclusive cross sections can be inferred from the model predictions: even if impact parameters from 0 to 8 fm have been considered in the BNV + Gemini calculations (see Fig. 3), the results filtered by the acceptance of the apparatus show that, due to the minimum detection angle, the contribution from impact parameters $b > 6$ fm is negligible.

4. Exclusive data

Focusing the analysis on the coincidence events with multiplicity three and four, we note that the impact parameters giving the largest contribution to the three and four-fold events are $b \approx 5$ fm. In this case two sources (see Fig. 3) with sufficiently high excitation energy and angular momentum are formed and at least one of them undergoes a binary decay.

A confirmation that three-fold events can be associated to central and medium impact parameters can be obtained studying the observable Y_{33}, first proposed in

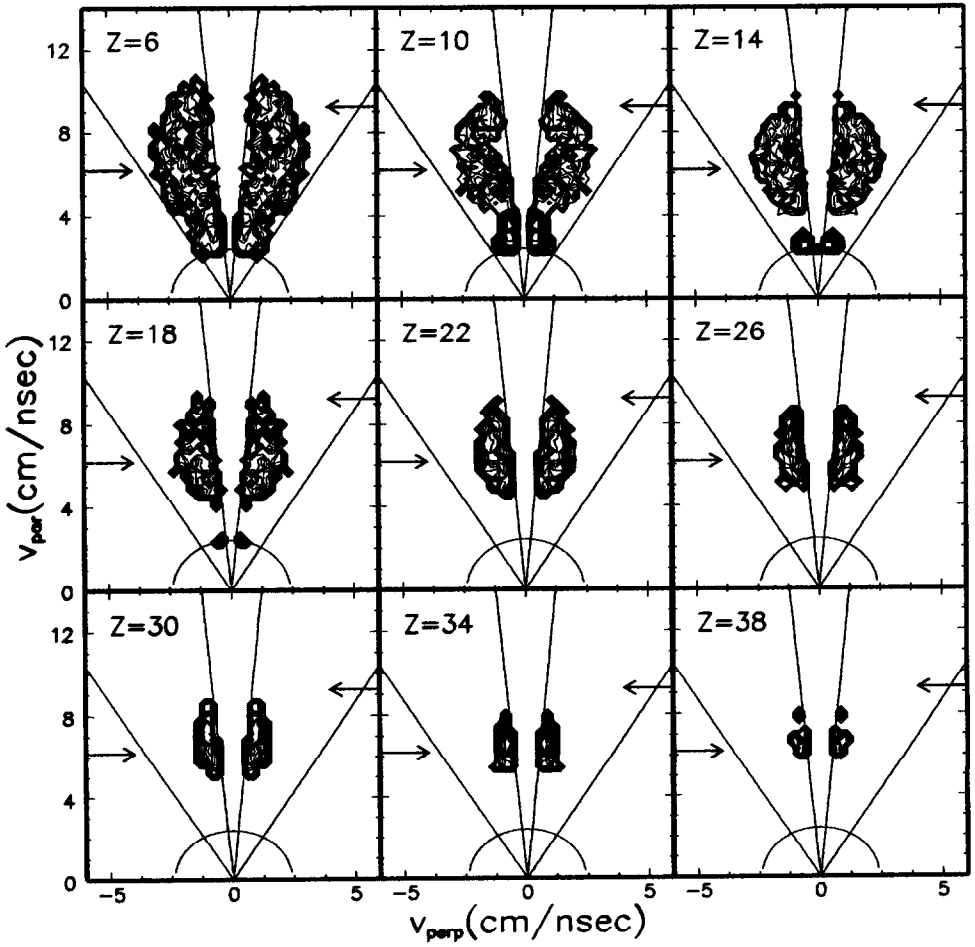

Fig. 4. Logarithmic contour plots of the parallel ($v_{\parallel}$) versus perpendicular ($v_{\perp}$) velocity for the events calculated in the BNV+Gemini approach. The description of arrows and contour lines is given in the caption of Fig. 2.

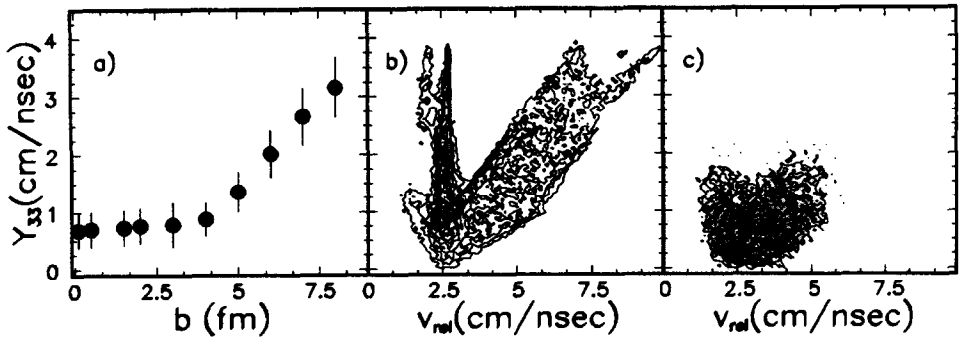

Fig. 5. (a) Y_{33} (cm/ns) versus b(fm) as predicted by BNV + Gemini calculations. (b) Linear contour plot of the predicted Y_{33} versus v_{rel} for the three-fold events; each event gives one Y_{33} value and three v_{rel} values. (c) Linear contour plot of the experimental Y_{33} versus v_{rel} for the three-fold events. The description of contour lines is given in the caption of Fig. 2.

ref. [17]. Y_{33} is defined in an event-by-event analysis as the maximum deviation of relative velocities from their mean value:

$$Y_{33} = \langle v_{rel} \rangle - v_{rel}^{min}, \tag{2}$$

where $\langle v_{rel} \rangle$ is the mean value of the three relative velocities in a given event and v_{rel}^{min} is the minimum relative velocity in the same event. A large value of Y_{33} indicates a wide dispersion of relative velocities which suggests peripheral events; on the other hand a low value of this observable is an indication of a common source for the detected fragments.

Fig. 5a shows the plot of Y_{33}, predicted by BNV + Gemini, as a function of the impact parameter. A strong correlation between Y_{33} and b is evident for the mid-peripheral impact parameters ($b \geqslant 5$ fm). The corresponding events lie, in the Y_{33} versus v_{rel} plot, in the two ridges of high Y_{33} (Fig. 5b). The branches are associated with fission fragments of a projectile-like residue in coincidence with a slow target-like fragment, i.e. with the fragments from the two sources formed at non-central impact parameters [6,15] when treating the entrance-channel dynamics via the BNV equation. The experimental contour plot is shown in Fig. 5c. The ridges corresponding to more peripheral reactions are not present: the measured three-fold events can thus be classified as produced in reactions where the impact parameters are smaller than 5 fm.

Further information on the impact parameters can be obtained analyzing the Z correlation and the angular and velocity distributions of the three-fold events.

From the charge-correlation plot [18,6] (Z_{min}/Z_{tot}, Z_{max}/Z_{tot}) shown in Fig. 6a, it appears that, for the measured reaction and for the angular acceptance of the apparatus, the production of three fragments of nearly-equal mass (upper corner), is the favourite exit channel for the deexcitation mechanism.

The total fragment charge Z_{tot} of the three-fold events, shown in Fig. 6b, has a gaussian shape. No significant tail, typical of a partial detection of the events [5],

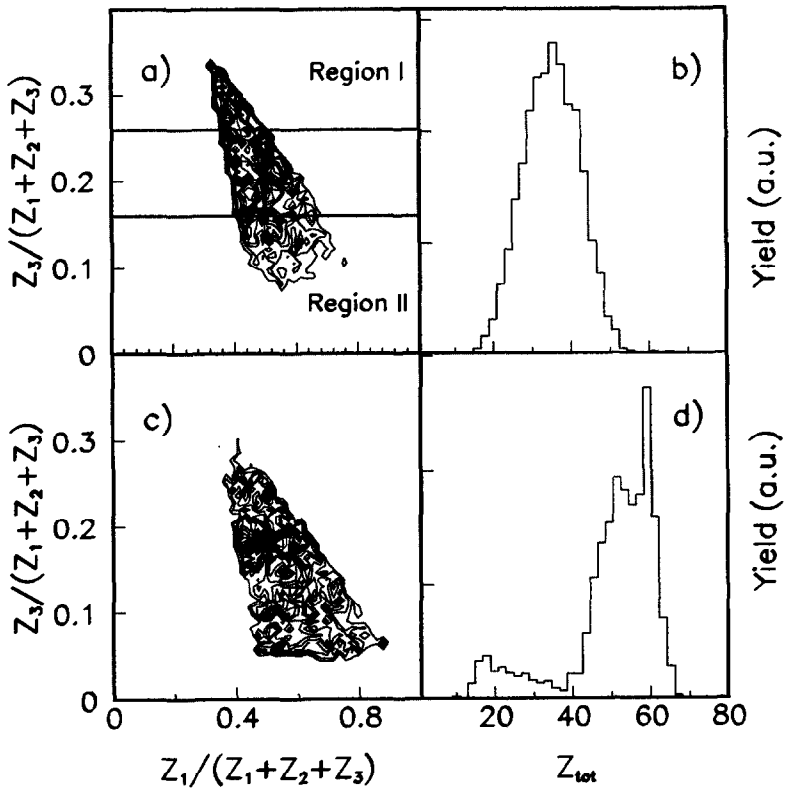

Fig. 6. (a) Linear contour plot of $Z_{min}/(Z_1+Z_2+Z_3)$ versus $Z_{max}/(Z_1+Z_2+Z_3)$ for three-fold events ($Z_1 \geq Z_2 \geq Z_3$). The lines delimitate the regions I and II as explained in the text. (b) Sum of the charges of all IMFs detected in three-fold events. (c) Linear contour plot of $Z_{min}/(Z_1+Z_2+Z_3)$ versus $Z_{max}/(Z_1+Z_2+Z_3)$ for three-fold events predicted by the BNV+Gemini approach. (d) Sum of the charges of the IMFs for three-fold events predicted by the BNV+Gemini approach. The predictions have been filtered by the acceptance of the apparatus. The description of contour lines is given in the caption of Fig. 2.

can be seen at low Z values. We are thus confident that most of the detected three-fold events do not come from higher multiplicities.

As already pointed out in ref. [6], the predictions of the BNV + Gemini coupling, shown in Figs. 6c and d do not reproduce both the charge correlation and the Z_{tot} spectrum, even arbitrarily increasing the excitation energy of the sources. This is an indication that the binary deexcitation mechanism is not adequate to reproduce our data.

We investigated the two extreme regions of Fig. 6a:

Region I–above the line $Z_{min}/Z_{tot} = 0.26$, corresponding to events with three nearly-equal mass fragments;

Region II–below the line $Z_{min}/Z_{tot} = 0.16$, corresponding to events where at least a pair of IMFs is very asymmetric in mass.

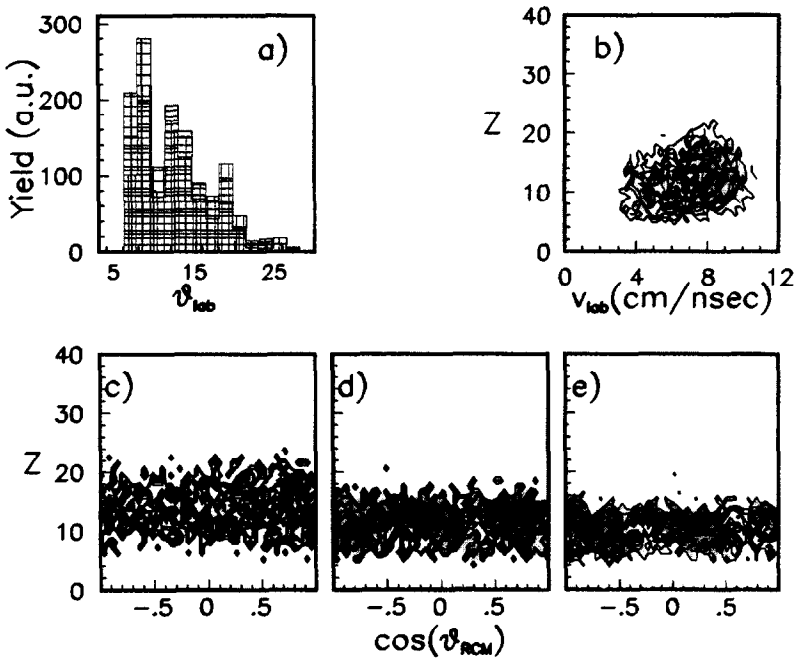

Fig. 7. Events of region I of Fig. 6a. (a) Laboratory emission angles (deg) of the fragments. For statistical reasons the events are grouped in 1.7° bins. The red histogram refers to Z_1, the blue to Z_2 and the green to Z_3. (b) Linear contour plot of the charge of the IMFs versus their laboratory velocity. Linear contour plot of the charge of the IMFs versus cos $\theta_{r.c.m.}$ for (c) heavier, (d) intermediate and (e) lighter fragments, respectively. The description of contour lines is given in the caption of Fig. 2.

The data of the remaining region, between the two lines just mentioned, have an intermediate behaviour with respect to the data of regions I and II and they will not be discussed further.

The relevant differences between the data of regions I and II, as far as the angular and velocity distributions are concerned, are hereafter considered.

(i) The angular distributions in the laboratory system are shown in Figs. 7a and 8a for the regions I and II, respectively. The three nearly-equal IMFs have a similar angular distribution, while the heaviest fragment of the region II, in contrast with the other two, is forward peaked.

(ii) In Figs. 7b and 8b the Z versus v_{lab} correlations are shown. Two bumps are clearly seen for the events of the region II. The first, around ≈ 5 cm/ns, is below the c.m. velocity (6 cm/ns). The corresponding fragments, traveling in the c.m. frame in opposite direction with respect to the beam, can thus be associated to target residues (TLF). The second bump is located around the beam velocity and accounts for projectile-like fragments (PLF). The low-velocity component is completely missing in the data of region I, giving an indication that the corresponding fragments have in average not only the same mass, but also the same laboratory velocity.

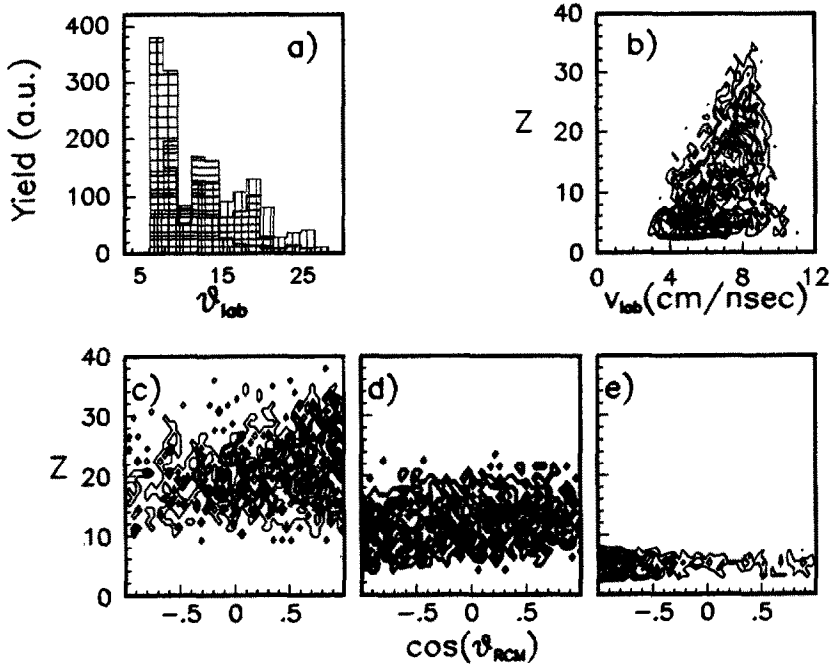

Fig. 8. Events of region II of Fig. 6a. (a) Laboratory emission angles (deg) of the fragments. The red histogram refers to Z_1, the blue to Z_2 and the green to Z_3. (b) Linear contour plot of the charge of the IMFs versus their laboratory velocity. Linear contour plot of the charge of the IMFs versus cos $\theta_{r.c.m.}$ for (c) heavier, (d) intermediate and (e) lighter fragments, respectively. The description of contour lines is given in the caption of Fig. 2.

(iii) An even clearer insight on the different behaviour of the events from regions I and II is provided by observing the Z distributions as a function of cos $\theta_{r.c.m.}$, $\theta_{r.c.m.}$ being the emission angle of the fragments in the recoil center of mass system. The c.m. velocity has been calculated as

$$V_{rec} = \frac{\Sigma A_i \times V_i}{\Sigma A_i}, \tag{3}$$

where the mass of the fragments is given by Eq. (1). For the events in region I, Eq. (3) gives a mean value for V_{rec} very similar to the one predicted by the incomplete-fusion systematics [19] (≈ 7.3 cm/ns), corresponding to a linear momentum transfer of 80%. Furthermore, the V_{rec} spectrum has a gaussian distribution, indicating an almost complete independence from the entrance channel [20]. For the events in region I, Figs. 7c, d and e show that the angular distributions are almost flat, indicating an isotropic emission in the recoil system and a global equilibrium reached in the reaction. For the events in region II (Figs. 8c, d and e) the heaviest and the lightest fragments are forward and backward peaked, respectively; this again suggests that the heaviest fragment is a PLF and the lightest is a TLF coming from peripheral impact parameters. This can be interpreted as a

signal that the selection based on Y_{33} does not completely exclude mid-peripheral reactions [17]. The predictions of BNV + Gemini [6,15] show that central impact parameters lead to nearly-isotropic angular distributions, whereas noncentral events ($b \geqslant 3$ fm) give forward and backward peaks for the heaviest and lightest fragments, respectively.

From (i), (ii), (iii) it appears reasonable to conclude that the experimental data of region I can be associated to central-impact parameters ($b = 0$–2 fm) and that the events of region II mainly come from intermediate b values (3–5 fm). We note that the charge partition, the angular and velocity distributions of the three-fold events of region II can be qualitatively well explained by BNV + Gemini, while for central-impact parameters the enhancement for the three equal masses is completely missing.

We considered up to now the impact-parameters selection and now we focus our attention on the emission mechanism.

As discussed in a previous paper [8], fragment–fragment relative-angle and relative-velocity distributions are quite sensitive to distinguishing between a prompt multi-fragmentation and a chain of sequential binary decays; a broad relative-angle distribution, extending up to $\theta_{rel} \approx 180°$ is obtained for a long lifetime sequential decay. For a simultaneous multifragmentation of an expanded and hot source in three IMFs with nearly the same mass or for sequential decays with lifetimes $\leqslant 10^{-22}$ s, one obtains a peak in the plot v_{rel}–θ_{rel} at $\theta_{rel} \approx 120°$ and $v_{rel} \approx 3.1$ cm/ns, corresponding to a Coulomb-like disassembly process.

The plots of the relative velocities as a function of the relative angles for the events of regions I and II are shown in Figs. 9a and b, respectively. The experimental data of region I show the enhancement at $\theta_{rel} \approx 120°$ and $v_{rel} \approx 3.2$ cm/ns, as predicted by a simultaneous emission; the events of region II have opposite emission velocities, again suggesting that the excited system sequentially decays or that these fragments come from the projectile and from the target, respectively.

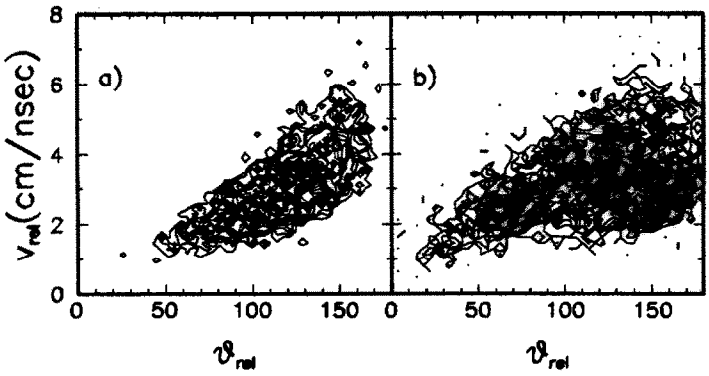

Fig. 9. (a) Linear contour plot of the experimental v_{rel} (cm/ns) versus θ_{rel} (deg) for the fragments in region I. (b) Linear contour plot of the experimental v_{rel} (cm/ns) versus θ_{rel} (deg) for the fragments in region II. The description of contour lines is given in the caption of Fig. 2.

These considerations and the disagreement between data and calculations (Fig. 6) are evidences that sequential binary decays are not experimentally seen for the most central-impact parameters.

In order to investigate if the enhancement at $\theta_{rel} \approx 120°$ could be due also to a partial detection of events with higher multiplicity, we performed a calculation of the simultaneous multifragmentation of an expanding source [8] with IMF multiplicity four. The results of these calculations are compatible with the experimental θ_{rel}, v_{rel} and V_{rec} values, only if the fourth (not detected) IMF has a maximum value $Z \approx 6$ and an emission angle $\approx 0°$. The probability of this occurrence is, however, negligible if the four-fold events have an isotropic emission as the three-fold ones.

We therefore analyzed the four-fold data, even if only a few hundred events have been collected in this measurement. A behaviour similar to the one of the three-fold events of region I has been found: the events lie in the upper region of the charge triangular plot, the angular distributions are almost flat and the recoil velocity has a mean value of ≈ 7 cm/ns, corresponding even in this case to a linear momentum transfer of $\approx 80\%$. This is an indication that three-fold events of the region I and four-fold events have a common origin, are formed at central impact parameters and are not due to higher-multiplicity events not completely detected.

In conclusion, from the analysis of the exclusive data, it appears that events coming from central collisions are consistent with a prompt multifragmentation mechanism.

In this respect it is worthwhile to mention that the enhanced cross section for fragments with nearly-equal masses has been indicated [21] as a signature for the occurrence of a simultaneous multifragmentation and that these central events could be exploited to investigate the formation and the decay of metastable nuclei of exotic shapes (toroidal, bubbles, etc.) [22].

5. Comparison with a multifragmentation model

In the previous section indications were found of a non-binary-sequential decay of the hot sources formed at central-impact parameters. To have a deeper understanding on the production of the observed fragments, we compared the experimental data with the prediction of the statistical multifragmentation model by Gross et al. [2,23], which describes the multiple disassembly of the expanded hot nuclear system: the fragmentation is given by the available phase space at the freeze-out volume.

The Berlin model has been successfully used at higher energies [24]; we note that the excitation energies of the heavy residues therein quoted are very similar to ones found by the BNV calculation [6] for the reaction we studied.

Since the necessary condition for using the statistical model is the establishment of a thermalized source, and since the agreement between the inclusive data and the BNV + Gemini predictions is an indication that the characteristics of the

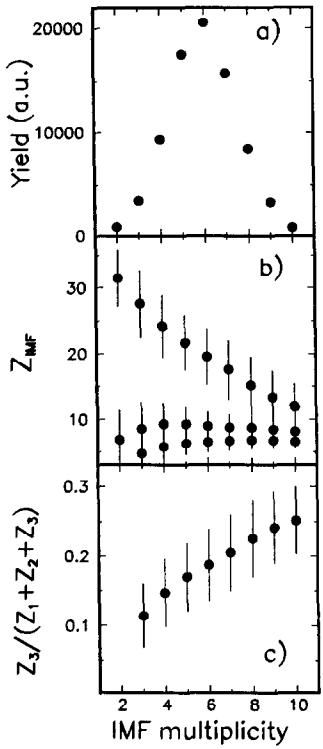

Fig. 10. Predictions of the multifragmentation model. (a) Multiplicity distribution; (b) Plot of the charge of the three largest fragments ($Z_1 \geqslant Z_2 \geqslant Z_3$) as a function of the IMF multiplicity; (c) Ratio of $Z_3/(Z_1+Z_2+Z_3)$ as a function of the IMF multiplicity ($Z_3/(Z_1+Z_2+Z_3) \approx 0.3$ means $Z_1 \approx Z_2 \approx Z_3$).

sources are correctly calculated, the input parameters given by the BNV calculations were used for the statistical multifragmentation code. Also in this case we used, as indicators of the agreement between data and predictions, the ratio Z_{min}/Z_{tot} (which reaches the value $\frac{1}{3}$ for three equal-charge fragments), the Z_{tot} spectrum and mean values of the charges of the three heaviest fragments (Z_1, Z_2, Z_3).

It is important to notice that the reproduction of the mass partition (Z_1, Z_2, Z_3, Z_{tot}, Z_{min}/Z_{tot}) is nontrivial; in fact it strongly depends on the excitation energy and cannot be obtained with the sequential-binary-decay model, for any value of the input quantities.

The first calculations have been made for zero angular momentum where BNV predictions give an excitation energy $E^* \approx 5$ MeV/u. The predicted IMF multiplicities, the charge of the three heaviest fragments and the ratio Z_{min}/Z_{tot} are reported in Fig. 10. The charge Z_1 of the heaviest fragment decreases from ≈ 30 to ≈ 10 for increasing multiplicity, while the other charges Z_2 and Z_3 are nearly independent from the multiplicity ($Z_2 \simeq Z_3 \simeq 7$–8). The value $Z_{min}/Z_{tot} \approx \frac{1}{3}$ is

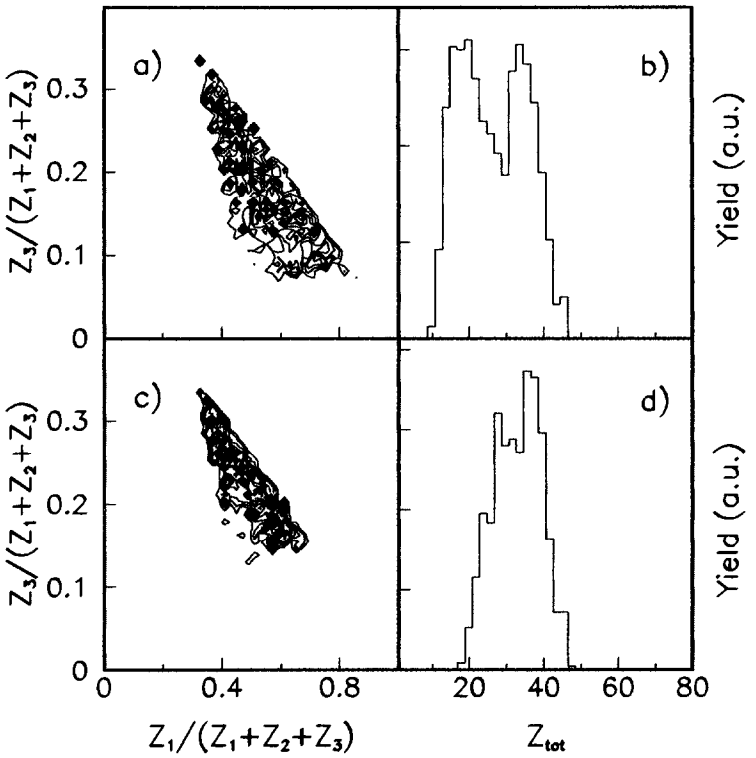

Fig. 11. Predictions of the multifragmentation model, filtered by the acceptance of the apparatus. (a) Linear contour plot of the $Z_{min}/(Z_1+Z_2+Z_3)$ versus $Z_{max}/(Z_1+Z_2+Z_3)$ for three-fold events; (b) Sum of the charges of the IMFs for three-fold events; (c) Linear contour plot of the $Z_{min}/(Z_1+Z_2+Z_3)$ versus $Z_{max}/(Z_1+Z_2+Z_3)$ for three-fold events with the constraint $Z \geqslant 6$. (d) Sum of the charges of the IMFs for three-fold events with the constraint $Z \geqslant 6$. The description of contour lines is given in the caption of Fig. 2.

reached for very high IMF multiplicities and for Z_1, Z_2 and Z_3 values smaller than the experimental ones.

In order to properly compare the predictions to the experimental data, the results of the calculations have been filtered by the acceptance of the apparatus. Figs. 11a and b show the charge-correlation plot and Z_{tot} distribution for the events detected as three-fold events, independently from the initial multiplicity. Fig. 11a shows that the upper corner of the Z-correlation *triangle* is no more empty as in Fig. 6c. The Z_{tot} distribution (Fig. 11b), not gaussian as the experimental one, shows two peaks, one at $Z_{tot} \simeq 36$, in agreement with experimental data, and the second at $Z_{tot} \simeq 17$, due the partial detection of higher-multiplicity events. As already pointed out, no evidence for this component can be found in the experimental distribution.

In order to see the role of the input parameters on the results of the calculations, both the excitation energy and the angular momentum were varied. The

excitation energy was increased up to ≈ 8 MeV/u, as suggested by the incomplete-fusion hypothesis [5]. The charge-correlation plot for the highest excitation energy is very similar to the one presented in Fig. 11a, whereas the Z_{tot} peak is down-shifted to 20. Excitation energies less than 5 MeV/u give a Z_{tot} peak shifted to values higher than 36. The peak at $Z_{tot} \approx 36$, in agreement with experimental data, is thus obtained only for the excitation energy is given by BNV calculations at $b = 0$ fm.

A further calculation for angular momentum $L = 70\hbar$, corresponding to an impact parameter $b = 3$ fm and an excitation energy $E^* \simeq 4$ MeV/u, gives IMF multiplicities smaller than in the previous calculations and closer to the experimental values. The most probable IMF multiplicity is around three, but the charges of the three heaviest fragments are very different from the experimental values: Z_1 is considerably higher ($Z_1 \approx 20$–35) and Z_2, Z_3 smaller ($Z_2 = Z_3 \approx 4$–5).

From all these calculations it results that, for any reasonable input in central collisions, the partition of three nearly-equal IMFs of $Z \simeq 12$ cannot be reproduced with the probability experimentally found. On the other side two results are promising in the multifragmentation model predictions:

(1) the nonnegligible presence of events in the upper part of the charge-correlation plot (Fig. 11a);

(2) the agreement with the experimental Z_{tot} distribution for the peak at ≈ 36, neglecting the events from higher multiplicities.

The discrepancies between data and multifragmentation predictions can be due to an underestimate of the evaporation and/or to the fact that the partition function could be different from the one successfully used by this statistical model at higher energies. To have an insight on this subject we finally compared the experimental data to the theoretical predictions, arbitrarily reducing the IMF multiplicity, i.e. disregarding in the predicted events all the fragments with $Z \leqslant 5$. With this constraint the resulting charge-correlation plot and Z_{tot} distribution, presented in Figs. 11c and d, respectively, are very similar to the experimental distributions, indicating that a statistical and simultaneous multifragmentation model could reproduce the most interesting features of the experimental data, like the enhancement for the production of three nearly-equal fragments, provided that some ingredients of the calculations could be properly modified.

6. Conclusions

In this paper we have analyzed IMF production in the $^{129}Xe + {}^{nat}Cu$ reaction at 45 MeV/u. We have focused our analysis on the three-fold coincidences and we have observed that different sets of events in the mass-correlation *triangle* (Fig. 6a), namely regions I and II of high- and low-charge asymmetry, come from reactions at different impact parameters. The angular and velocity analysis shows that the events with three nearly-equal fragments (region I) seem to correspond to very central collisions ($b \leqslant 2$). The relative velocities and angles of these IMFs are typical of a simultaneous multifragmentation of an expanding hot source. The

three-fold events of region II, on the contrary, seem to come from more peripheral collisions ($b \geqslant 3$); the argument relies on the similarity of these fragments with the projectile and the target as far as the angular and velocity distributions are concerned.

We have compared our data with two different deexcitation models following a BNV dynamical calculation, namely a sequential-decay [7] and a prompt multifragmentation [2] model. The good agreement for the inclusive data and the consequences of varying the excitation energy with respect to BNV predictions indicate that the values of the size and excitation energies of the sources are correctly predicted by the BNV calculations. The production of the events of the region I cannot be due to a sequential binary deexcitation of the hot nuclei formed in the central collisions: the distributions of the relative velocities and angles for the fragments lying in this region clearly demand a prompt multifragment emission, and some promising agreement with the statistical model by Gross et al. [2] is found, even if it is not yet satisfactory.

Acknowledgements

The authors would like to thank A. Bonasera, M. Cavinato and M. Di Toro for many interesting and stimulating discussions. The technical assistance of R. Bassini, C. Boiano, S. Brambilla, G. Busacchi, A. Cortesi, M. Malatesta and G. Sava is gratefully acknowledged. This work has been supported in part by funds of the Italian Ministry of University and Scientific Research.

References

[1] X. Campi, Phys. Lett. B208 (1988) 351;
X. Campi and H. Krivine, Z. Phys. A344 (1992) 81;
J. Randrup and S.E. Koonin, Nucl. Phys. A356 (1981) 223;
J.P. Bondorf, Nucl. Phys. A387 (1982) 25c

[2] D.H.E. Gross, X. Zhang and S. Xu, Phys. Rev. Lett. 56 (1986) 1544;
X.Z. Zhang, D.H.E. Gross, S. Xu and Y.M. Zheng, Nucl. Phys. A461 (1987) 668;
D.H.E. Gross, Rep. Prog. Phys. A53 (1990) 605

[3] See for instance H.W. Barz, J.P. Bondorf, R. Donangelo, R. Elmer, F.S. Hansen, B. Jakobsson, L. Karlsson, H. Nifeneker, H. Schulz, F. Schussler, K. Sneppen and K. Söderström, Nucl. Phys. A531 (1991) 453;
J. Peter, Workshop on dynamical fluctuations and correlations in nuclear collisions, Aussois, March 1992, Nucl. Phys. A545 (1992) 173c;
L. Phair, D.R. Bowman, C.K. Gelbke, W.G. Gong, Y.D. Kim, M.A. Lisa, W.G. Lynch, G.F. Peaslee, R.T. de Souza, M.B. Tsang and F. Zhu, Nucl. Phys. A548 (1992) 489;
D.R. Bowman, C.M. Mader, G.F. Peasle, W. Bauer, N. Carlin, R.T. de Souza, C.K. Gelbke, W.C. Gong, Y.D. Kim, M.A. Lisa, W.G. Lynch, L. Phair, M.B. Tsang, C. Williams, N. Colonna, K. Hanold, M.A. McMahan, G.J. Wozniak, L.G. Moretto and W.A. Friedman, Phys. Rev. C46 (1992) 1834

[4] M.B. Tsang, G.F. Bertsch, W.G. Lynch and M. Tohyama, Phys. Rev. C40 (1989) 1685;
C. Cavata, M. Demoulins, J. Gosset, M.C. Lemaire, D.L'Hote, J. Poitou and O. Valette, Phys. Rev. C42 (1990) 1760;

D.R. Bowman, G.F. Peasle, N. Colonna, R.J. Charity, M.A. McMahan, D.N. Delis, H. Han, K. Jing, G.J. Wozniak, L.G. Moretto, W.L. Kehoe, B. Libby, A.C. Mignerey, A. Moroni, S. Angius, I. Iori, A. Pantaleo and G. Guarino, Nucl. Phys. A523 (1991) 386

[5] P. Roussel Chomaz, N. Colonna, Y. Blumenfeld, B. Libby, G.F. Peasle, D.N. Delis, K. Hanold, M.A. McMahan, J.C. Meng, Q.C. Sui, G.J. Wozniak, L.G. Moretto, H. Madani, A.A. Marchetti, A.C. Mignerey, G. Guarino, N. Santoruvo, I. Iori and S. Bradley, Nucl. Phys. A551 (1993) 508

[6] M. Bruno, M. D'Agostino, M.L. Fiandri, E. Fuschini, P.M. Milazzo, A. Cunsolo, A. Foti, F. Gramegna, F. Gulminelli, I. Iori, L. Manduci, A. Moroni, R. Scardaoni, P. Buttazzo, G.V. Margagliotti, G. Vannini, G. Auger and E. Plagnol, Phys. Lett. B292 (1992) 251

[7] R.J. Charity, M.A. McMahan, G.J. Wozniak, R.J. McDonald, L.G. Moretto, D.G. Saranties, L.G. Sobotka, G. Guarino, A. Pantaleo, L. Fiore, A. Gobbi and K.D. Hildebrand, Nucl. Phys. A483 (1988) 371

[8] M. Bruno, M. D'Agostino, M.L. Fiandri, E. Fuschini, P.M. Milazzo, A. Cunsolo, A. Foti, F. Gramegna, I. Iori, L. Manduci, A. Moroni, P. Buttazzo, G.V. Margagliotti and G. Vannini, Nuovo Cimento 105A (1992) 1629

[9] I. Iori, L. Manduci, A. Moroni, R. Scardaoni, S.C. Wen, Z. Yuzhao, Z. Guangming, F. Giglio, E. Mora, G. Di Pietro, L. Dellera, A. Cortesi, R. Bassini, C. Boiano, S. Brambilla, M. Malatesta, M. Bruno, M.D'Agostino, M.L. Fiandri, E. Fuschini, P.M. Milazzo, G. Busacchi, A. Cunsolo, A. Foti, G. Sava, F. Gramegna, P. Buttazzo, G.V. Margagliotti and G. Vannini, Nucl. Instr. Meth. A325 (1993) 458

[10] M. Bruno, M. D'Agostino, M.L. Fiandri, E. Fuschini, P.M. Milazzo, S. Ostuni, F. Gramegna, I. Iori, L. Manduci, A. Moroni, R. Scardaoni, P. Buttazzo, G.V. Margagliotti and G. Vannini, Nucl. Instr. Meth. A311 (1992) 189

[11] N. Colonna, G.J. Wozniak, A. Veeck, W. Skulski, G.W. Goth, L. Manduci, P.M. Milazzo and P.F. Mastinu, Nucl. Instr. Meth. A321 (1992) 529

[12] P.F. Mastinu, P.M. Milazzo, M. Bruno, M. D'Agostino and L. Manduci, Nucl. Instr. Meth. 338 (1994) 419

[13] R.J. Charity, D.R. Bowman, Z.H. Liu, R.J. Mac Donald, M.A. McMahan, G.J. Wozniak, L.G. Moretto, S. Bradley, W.L. Kehoe and A.C. Mignerey, Nucl. Phys. A476 (1988) 516

[14] D.R. Bowman, G.F. Peasle, N. Carlin, R.T. de Souza, C.K. Gelbke, W.C. Gong, Y.D. Kim, M.A. Lisa, W.G. Lynch, L. Phair, M.B. Tsang, C. Williams, N. Colonna, K. Hanold, M.A. McMahan, G.J. Wozniak and L.G. Moretto, Phys. Rev. Lett. 70 (1993) 3534

[15] A. Bonasera, M. Cavinato, M. Colonna, N. Colonna, M. D'Agostino, M. Di Toro, E. Fuschini, F. Gulminelli and L.G. Moretto, XXIX Int. Winter Meeting on nuclear physics, Bormio, January 1991, ed. I. Iori, p. 193, and references therein;
M. Colonna, N. Colonna, A. Bonasera and M. Di Toro, Nucl. Phys. A541 (1992) 295

[16] M. Bruno, M. D'Agostino, P.M. Milazzo, S. Ostuni, E. Fuschini and A. Moroni, Nucl. Instr. Meth. A305 (1991) 410

[17] M. Louvel, G. Bizard, R. Bougault, R. Brou, E. Buta, D. Durand, A. Genoux-Lubain, A. Hajfani, T. Hamdani, J.L. Laville, C. Le Brun, J.F. Lecolley, J.P. Patry, J. Peter, N. Prott, R. Regimbart, J.C. Steickmeier, B. Tamain, A. Badala, H. Doubre, Y. El-Masri, H. Fugiwara, K. Hagel, F. Hanappe, S. Jeong, G.M. Jin, S. Kato, S. Lee, T. Matsuse, T. Motobayashi, A. Peghaire and F. Saint-Laurent, XXX Int. Winter Meeting on nuclear physics, Bormio, January 1992, ed. I. Iori, p. 11

[18] H.R. Jaqaman, G. Papp and D.H.E. Gross, Nucl. Phys. A514 (1990) 327

[19] V.E. Viola Jr., B.B. Back, K.L. Wolf, T.C. Awes, C.K. Gelbke and H. Breuer, Phys. Rev. C26 (1982) 178

[20] O. Lopez, M. Aboufiriassi, A. Badala, B. Bilwes, R. Bougault, R. Brou, J. Colin, F. Cosmo, D. Durand, A. Genoux-Lubain, D. Horn, J.L. Laville, C. Le Brun, J.F. Lecolley, F. Lefebvres, M. Louvel, M. Mahi, C. Paulot, A. Peghaire, G. Rudolf, F. Scheibling, J.C. Steickmeier, L. Stuttge, B. Tamain and S. Tomasevic, Phys. Lett. B315 (1993) 34

[21] H.M. Xu, J.B. Natowitz, C.A. Gagliardi, R.E. Tribble, C.Y. Wong and W.G. Lynch, Phys. Rev. C48 (1993) 933

[22] M. Bruno, M. D'Agostino, M.L. Fiandri, E. Fuschini, P.F. Mastinu, P.M. Milazzo, F. Gramegna,

A.M.J. Ferrero, F. Gulminelli, I. Iori, A. Moroni, G.V. Margagliotti, G. Vannini and E. Plagnol, in preparation

[23] A.R. De Angelis and D.H.E. Gross, Comput. Phys. Commun. 76 (1993) 113

[24] C.A. Ogilvie, J.C. Adloff, M. Begemann-Blaich, P. Boissou, J. Hubele, G. Imme, I. Iori, P. Kreutz, G.J. Kunde, S. Leray, V. Lindenstruth, Z. Liu, U. Lynen, R.J. Meijer, U. Milkau, W.F. Müller, C. Ngô, J. Pochodzalla, G. Raciti, G. Rudolph, H. Sann, A. Schüttauf, W. Seidel, L. Stuttge, W. Trautmann and A. Tucholski, Phys. Rev. Lett. 67 (1991) 1214;
B.A. Li, A.R. De Angelis and D.H.E. Gross, Phys. Lett. B303 (1992) 225